J Polym Res (2012) 19:9950
DOI 10.1007/s10965-012-9950-1

ORIGINAL PAPER

Synthesis and characterization of p(NIPAM-AA-AAm) microgels for tuning of optical Properties of silver nanoparticles

Hina Naeem · Zahoor H. Farooqi · Luqman Ali Shah · Mohammad Siddiq

Received: 14 March 2012 / Accepted: 25 July 2012 / Published online: 15 August 2012

Abstract Three compositions of p(NIPAM-AA-AAm) terpolymer microgels with various AA content have been prepared by free radical emulsion polymerization. Silver nanoparticles were synthesized in these microgels by in-situ reduction method. The temperature sensitivity of terpolymer microgels and hybrid gels was investigated using dynamic laser light scattering technique at three different pH values. The hydrodynamic radius of the microgels as a function of pH at 20 and 50 °C was also studied by the same technique. The optical properties of silver nanoparticles (AgNPs) have been studied by UV-Visible and Photo-luminescence measurements at various conditions of pH and temperature. The pH and temperature sensitivity of microgels was compared with hybrid polymer microgels of the same monomer compositions. The equilibrium swelling ratios, volume phase transition temperature and critical transition pH of microgels and hybrid gels was found to be dependent on microgels composition. A two step volume phase transition was observed with high acrylic acid content in acidic conditions. The terpolymer microgels and hybrid gels become unstable at low pH and high temperature.

Keywords Microgels · Hybrid gels · Equilibrium swelling ratios · Dynamic laser light scattering · Volume phase transition temperature

Introduction

Over the last few years, there is an exciting new trend in nanoscience to develop novel multifunctional nano materials due to their promising applications in electronics and optical devices, biomedicine, catalysis, sensors and controlled drug delivery for therapy [1–3]. Inorganic metal nanoparticles (NPs) posses unique optical properties ranging from distance dependent, refractive index dependent, size dependent plasmon resonance and Raman enhancement to fluorescence. Due to these properties, these nanomaterials have been extensively used in biodiagnostic imaging [4], biological labeling [5], and sensing. An example of a device which is based on excitation of surface plasmon resonance (SPR) biosensors [6], in which optical scattering from a thin nanoparticle film is used as a sensitive indicator of refractive index changes due to molecular surface binding events. Nanomaterials with pH-responsive optical properties are gaining more attention due to their applications in the investigation of diseases such as cancer and cystic fibrosis [7]. However, nanomaterials tend to aggregate easily, causing difficulties for long term storage, processing and applications. Stabilizing agents such as micelles [8], latexes [9], and microgels [10] have been used to increase the stability of nanoparticles. The in-situ synthesis of NPs in these microbeads has two-fold advantages: the use of polymer sphere as microreactors and production of materials with structural hierarchy. In contrast to other templates, responsive polymer microgels have the advantages of simple synthesis and easy functionalization and fabrication of inorganic NPs in the pH-responsive polymers is one way

Electronic supplementary material The online version of this article (doi:10.1007/s10965-012-9950-1) contains supplementary material, which is available to authorized users.

H. Naeem · Z. H. Farooqi · L. A. Shah · M. Siddiq (✉)
Department of Chemistry, Quaid-I-Azam University,
Islamabad 45320, Pakistan
e-mail: m_sidiq12@yahoo.com

Z. H. Farooqi
Institute of Chemistry, University of the Punjab,
New Campus,
Lahore 54590, Pakistan

to make materials with pH-sensitive optical properties. The pH and temperature induced swelling/deswelling behavior of microgels has been reported previously [11, 12]. The integration of inorganic nanoparticles in different polymeric structures has also been reported recently [17, 36, 37, 39]. Biffis et al. [13, 14] have reported the catalytic applications of microgels-stabilized metal nanoparticles for different reactions and confirmed the enhanced catalytic activity of Pd nanostructures in Heck reaction of activated aryl bromides. Ionov et al. reported the fabrication of nanosensors based on CdSe NPs immobilized on the pH-responsive p(2-vinyl pyridine) brushes [15]. The same P2VP brushes were used for the immobilization of Ag NPs by Tokareva et al. [16]. The pH-induced shrinkage of P2VP chains caused a red shift of surface plasmon resonance bands of Ag NPs. Lu et al. have shown that the thermosensitive core/shell microgels, which are composed of a polystyrene core and a cross-linked p(N-isopropylacrylamide) PNIPAM shell, can be used as nanoreactors [19, 20]. Similarly, a p(N-isopropyl acrylamide-allylacetic acid) microgels was used by Liz-Marzan et al. for the synthesis of Au nanorods based core-shell structured hybrid materials [21]. However, all these methods require presynthesized NPs capped with functional ligands. Kumacheva's group first fabricated different types of NPs (CdS, Ag and Fe_3O_4) inside the NIPAM based microgels by in-situ template method [22–24]. He studied a wide range of composites with unique optical properties and structural hierarchy. Also, Suzuki and Kawaguche synthesized Au NPs in the PNIPAM microgels [17]. They found that the color of hybrid microgels is because of interparticle interactions of the nanoparticles which changes according to the swelling/deswelling behaviour of thermosensitive microgels. However, few studies have been reported for pH-sensitive optical property changes of inorganic NPs immobilized in the microgel templates. Kumacheva's group synthesized Ag NPs in pH-responsive microgels of poly (N-isopropylacrylamide-acrylic acid-2-hydroxyethyl acrylate) (p(NIPAM-AA-HEA)). During the study of Ag NPs based p(NIPAM-AA-HEA) hybrid microgels, he found that only the Ag NPs synthesized through photoreduction of Ag^+ ions were fluorescent, while the Ag NPs prepared from conventional reduction method were nonfluorescent. Wu et al. [36] also reported the fluorescent pH-sensitive hybrid gels based on the in-situ synthesis of Ag and Ag/Au bimetallic NPs in the interior of multiple sensitive p(NIPAM-AA-AAm) terpolymer microgels.

Here in, we present the in-situ synthesis of Ag NPs within the p(NIPAM-AA-AAm) terpolymer microgels with different mole ratio of AA and NIPAM using conventional reduction method. Different techniques including FT-IR, dynamic light scattering, UV–vis spectroscopy and fluorescence spectroscopy were used to characterize both pure and hybrid microgels. The aim of the present work is not only to study the effect of AA content on temperature and pH-sensitivity of pure and hybrid microgels but also to tune the optical properties of Ag NPs by varying the solution pH as well as by varying the AA content.

Experimental part

Materials N, N-methylenebisacrylamide (BIS) was obtained from Acros and all other chemicals were purchased from Aldrich. N-isopropylacylamide (NIPAM) was recrystallized from hexane-toluene (1:1 volume ratio) mixture and dried in a vacuum. Acrylic acid (AA) was purified through distillation under reduced pressure. N, N-methylenebisacrylamide (BIS), ammonium persulphate (APS) and sodium dodecyl sulphate (SDS), Acrylamide (AAm), silver nitrate ($AgNO_3$), sodium borohydride ($NaBH_4$) were used as received. Deionized water was used for all reactions, solution preparation and microgels purification.

Microgel synthesis The microgels were synthesized by free radical emulsion polymerization of NIPAM, AAm, AA and BIS using APS as an initiator as reported previously [27, 36]. Three compositions of microgels were prepared by varying the amount of AA and NIPAM. The amount of materials used in the synthesis of these three compositions is given in Table 1. For each composition a mixture of NIPAM, AAm, AA, BIS and 0.0510 g SDS were added in 95 ml of deionized water in a 250 ml three-neck round-bottom flask equipped with a condenser, nitrogen gas inlet and a thermometer. The total number of moles of the components in all the microgels samples was kept constant at

Table 1 Feed composition of p(NIPAM-AA-AAm) terpolymer microgels particles

Sample code	Monomer used	Monomer mass[g]	Monomer moles $\times 10^4$	Total moles used	Mol-percentage
MG01	NIPAM	1.030	91.1	0.0105	87
	AA	0.022	3.1		3
	AAm	0.0373	5.2		5
	BIS	0.0809	5.3		5
MG02	NIPAM	0.9960	88.1	0.0105	84
	AA	0.0453	6.3		6
	AAm	0.0373	5.2		5
	BIS	0.0809	5.3		5
MG03	NIPAM	0.9610	85.0	0.0105	81
	AA	0.0680	9.4		9
	AAm	0.0373	5.2		5
	BIS	0.0809	5.3		5

0.0105. The mixture was continuously stirred and heated to 70 °C under N_2 purge. After 30 min, 5 ml of APS (0.05 M) was added in the reaction mixture to start the polymerization reaction. The reaction was carried out for 5 h. The prepared p(NIPAM-AA-AAm) terpolymer microgels were purified by centrifugation, decantation and washed with water. The resultant microgels was further purified by 7 days of dialysis (Spectra/Por molecular porous membrane tubing, cutoff 12 000–14 000) against very frequently changed water at room temperature to remove unreacted monomers.

In-situ synthesis of Ag NPs in p(NIPAM-AA-AAm) terpolymer microgels A series of hybrid microgels with Ag NPs immobilized inside were synthesized from same p(NIPAM-AA-AAm) microgels. 15 mL of microgels was added to 80 ml of deionized water in a 100 ml round bottom flask and then 0.008 g $AgNO_3$ was added in reaction mixture. This reaction mixture was stirred for 1 h in ice cold bath under N_2 purge. After that $NaBH_4$ solution (0.44 g in 5 ml water) was added dropwise to the reaction mixture. The reaction mixture was further stirred for 2 h. The resulting hybrid microgels loaded with Ag NPs were purified by decantation and 30 min dialysis against very frequently changed water. The hybrid gels were coded as HG01, HG02, and HG03.

Characterization The FTIR was used to identify different functional groups present in the microgels. The FTIR spectra of dried microgels were recorded with Fourier transform infrared spectrometer. The UV-Visible absorption spectra were obtained from Shindazu 1601 UV–vis spectrometer at different temperature and pH values. The PL spectra of hybrid microgels dispersions were performed on Perkin Elmer LS 55 Luminescence spectrometer at different pH values. The pH values were measured on a WTW Inolab pH 720 pH meter. The morphology of the hybrid microgel was studied using conventional JEOL SEM 5910-LV. Dynamic laser light scattering was performed on a standard laser light scattering spectrometer (Brookhaven Instruments) at an angle of 90°. A He-Ne laser (35 mW, 637 nm) was used as light source. All the microgels and hybrid gels were passed through Millipore Millex –HV filters with a pore size of 0.45 μm to remove any dust particles before performing measurements. The correlation functions were analyzed by constrained regularized CONTIN method to obtain distribution decay rates. The apparent diffusion coefficient is then obtained from these decay rates. The apparent diffusion coefficient is given by $D_{app}=\Gamma/q^2$ with scattering vector, $q = 4\pi n(\sin\theta/2)\lambda$ where n, λ and θ being the solvent refractive index, the wavelength of incident light and the scattering angle respectively. The hydrodynamic radius is calculated by using Stokes-Einstein equation, $R_h=k_BT/6\pi\eta D$ where T, k_B, and η are the absolute temperature, the Boltzmann constant, and the solvent viscosity respectively.

Results and discussion

The multi-sensitive p(NIPAM-AA-AAm) microgels were prepared by free radical emulsion polymerization of NIPAM, AA, and AAm by varying the content of AA and NIPAM using BIS as a crosslinker. The FTIR spectrum of p(NIPAM-AA-AAm) microgels shows different peaks at different positions for different functional groups. For amide group C = O a characteristic peak appeared at 1633.8 cm^{-1}, peak for N-H(bending) appeared at 1538.7 cm^{-1}, for C-N (stretching) peak appeared at 1366.9 cm^{-1}, for $–CH_2$- and -CH_3(bending) peaks appeared near 1456.0 and 1386.2 cm^{-1} respectively [18]. The broad and intense peak near 3289.9 cm^{-1} gives characteristic peak for N-H stretching showing the hydrogen bonding for water attached to polymer and confirms gel formation. Also, the SEM micrograph in Fig. 1 shows the morphology of prepared hybrid system.

Temperature sensitivity of p(NIPAM-AA-AAm) microgels at different pH values

The temperature sensitivity was studied at different pH values of 2.9, 4.3 and 8.2 in terms of change in R_h values measured at a scattering angle of 90°. The pH values of all the microgels dispersions were adjusted by using very dilute HCl and NaOH aqueous solutions. The NIPAM component in the p(NIPAM-AA-AAm) microgels network undergoes a volume phase transition from swollen to shrunken state by increasing temperature. The driving force for thermal sensitive volume phase transition was considered to be a balance between hydrophobic/hydrophilic interactions between network chains and water molecules [31, 32]. The hydrophilicity/hydrophobicity of the pendant groups in the microgels network can be controlled by changing the solution pH [27].

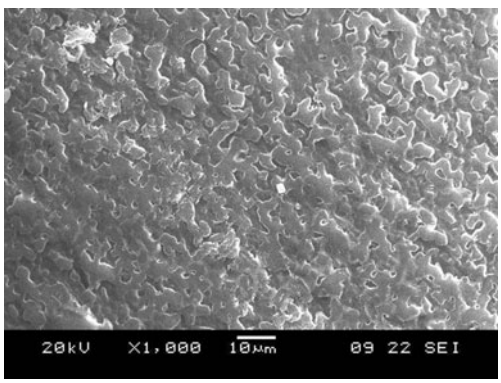

Fig. 1 SEM micrograph of HG01 at pH=4.3

The entropically favored expulsion of water from the polymer matrix along with hydrophobic and hydrogen-bonding interactions between neighboring polymer chains allow the particles to undergo a large-magnitude volume change [25, 26]. This transition is associated with decreasing solvency of water molecules for NIPAM component in the microgels [33].

Figure 2 shows the temperature induced transition of p(NIPAM-AA-AAm) microgels with different AA content at pH=2.9. The pK_a value of AA moiety in p(NIPAM-AA-AAm) microgels is 4.2 [34]. At low temperature, there is a greater degree of H-Bonding between water molecules and polymer chains. Upon increasing the temperature these forces of attraction becomes weak, dehydration occurred in the polymer network leading to shrinkage of microgels particles. However, at low pH of 2.9 collapsing is followed by aggregation of microgels particles. This is because of hydrophobic interactions which dominate at low pH and high temperature conditions [29].

Upon increasing the AA content the size of microgels particles decreases. This is because at low pH values of 2.9, AA groups cause hydrophobicity in the microgels network. Also, with decreasing AA content the extent of shrinkage decreases [31]. As a result aggregation is achieved at lower temperature in composition with high AA content. However, there is a very slight decrease in VPTT upon increasing AA content. In acidic conditions the size of aggregates also depends on the amount of AA in the microgels network. The higher the amount of AA moieties, the greater will be the size of aggregates [29].

Figure 3 shows the temperature dependence of average R_h values of p(NIPAM-AA-AAm) microgels with different AA content at pH=4.3. At pH=4.3 the AA moieties are partially ionized and the size of microgels is increased in comparison with microgels at pH=2.9. A pH-induced volume change is apparent at all temperatures along with broadening of the phase transition region and a decrease in the deswelling magnitude. These effects are due to both Coulombic repulsion between charged AA units and the

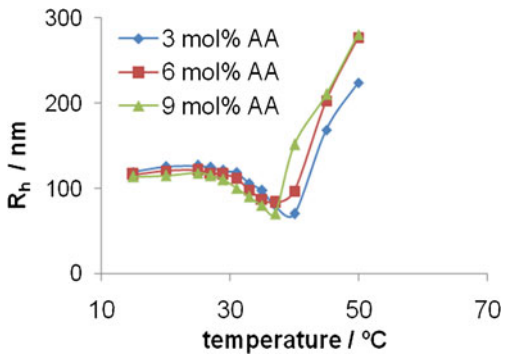

Fig. 2 Temperature dependence of average R_h values of pure microgels with different AA content at pH=2.9

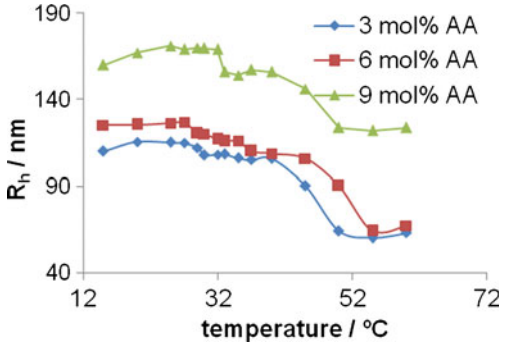

Fig. 3 Temperature dependence of average R_h values of pure microgels with different AA content at pH=4.3

increased osmotic pressure (Donnan potential) from the counterions [30]. Also, the transition shifts to slightly higher temperatures. However, at pH=4.3 a two-step volume phase transition is observed which becomes more pronounced with increasing AA content [29]. The initial shrinking occurs in a lower temperature range of 30–34 °C while the second transition proceeds to higher temperatures with a large volume change. This two-stage volume phase transition can be explained by considering the cross-linker heterogeneity among individual microgels particles. During particle growth, the cross-linker is statistically incorporated faster than other component monomers, resulting in radial distribution of cross linkers in the microgels. So, one can consider the individual microgels particle as having an internal core/shell type structure with respect to cross linking density, where the core represents the more densely cross- linked centre and the shell represents the relatively loosely cross-linked periphery [35, 36]. However this radial distribution of cross-linkers becomes less significant when the cross linking density is more than 7 mol % [35]. With increasing AA content, the intermediate plateau between two transitions becomes more pronounced. This is due to a larger decrease in local dielectric constant within the microgels particles as the water molecules are expelled from the network. At pH=4.3 no aggregation is observed beyond the critical transition temperature as compared to microgels at pH=2.9. The partial ionization of AA groups stabilizes the particles during collapsing process. Due to this stabilization microgels reach the equilibrated collapsing limit without aggregation.

Figure 4 shows the temperature dependence of average R_h values of p(NIPAM-AA-AAm) terpolymer microgels with different AA content at pH=8.2. All the particles are in maximum swollen state. The ionized AA groups increase VPTT to such an extent that no sharp transition is observed in the studied temperature range (≤55 °C). Introduction of AAm segment in the microgels network increases the hydrophilicity to a very large extent as compared to P(NIPAM-AA) polymer microgels network [36]. With

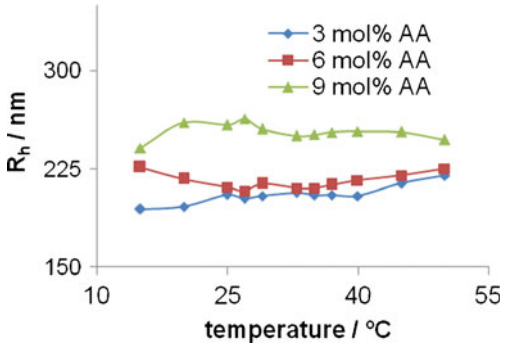

Fig. 4 Temperature dependence of average R_h values of pure microgels with different AA content at pH=8.2

increasing AA content the size of microgels particles increases which is shown by increase in hydrodynamic radius of particles. At high pH value of 8.2 the temperature sensitivity of microgels decreases and the pH effect becomes dominant.

pH sensitivity of p(NIPAM-AA-AAm) terpolymer microgels

pH sensitivity has been studied in terms of change in R_h values measured at two different temperature conditions of 20 and 50 °C. As expected, the functional AA groups in the terpolymer microgels network resulted in pH sensitivity. At pH values below the pK_a value of AA, the size of microgels remained almost constant. When the pH was above the pK_a value of AA, deprotonation of AA groups starts. At pH value greater than 6, all the AA units were ionized and a maximum swelling ratio is attained. The pH sensitivity of p(NIPAM-AA-AAm) microgels allows us not only to study the optical properties of Ag NPs immobilized inside the microgels network and to change the local surface environments but also to change the interaction degree between the drug and gel network chains to control the drug release [37].

Figure 5 shows the pH- induced volume phase transitions of p(NIPAM-AA-AAm) terpolymer microgels with different AA content at T=20 °C. All the microgels particles showed a continuous volume change in three stages with the increase in pH values of external media. First stage was observed below the pK_a value of AA groups in which the size of microgels remained nearly constant. The second stage was observed at pH≥4.2 in which the size of microgels particles increases abruptly. After that when the pH>6.5 the size of microgels particles becomes almost constant due to complete deprotonation of all the AA groups in the microgels network. All the three samples undergo pH sensitive volume phase transitions in three different stages. At higher pH values, the size of microgels with high AA content increases significantly as compared to the microgels with low AA content. However, the critical transition pH, which is around pH ≥4.2, remained almost same for all the compositions.

Figure 6 shows the pH sensitivity of p(NIPAM-AA-AAm) terpolymer microgels with different AA content at T=50 °C in which all the three stages were observed. However, at low pH values, the size of microgels particles with higher AA content increases as compared to microgels with low AA content. This is due to the aggregation of particles at higher temperature and lower pH values. Also, under high temperature conditions the pH sensitivity of microgels network is more significant as compared to that of lower temperature conditions. This is due to the presence of AAm segment in the microgels network. The AAm groups undergo hydrolysis into carboxylic acid groups and as a result the size of microgels increases [28].

When we compare the pH sensitivity of all the samples with different AA content at two different temperature conditions of 20 and 50 °C, the results indicate that under acidic conditions the size of microgels particles at 50 °C is smaller than that of at 20 °C. However, under basic conditions the size of microgels at 50 °C becomes significantly larger than at 20 °C. This increase is due to the hydrolysis of AAm segments into carboxylate groups. Also, the higher

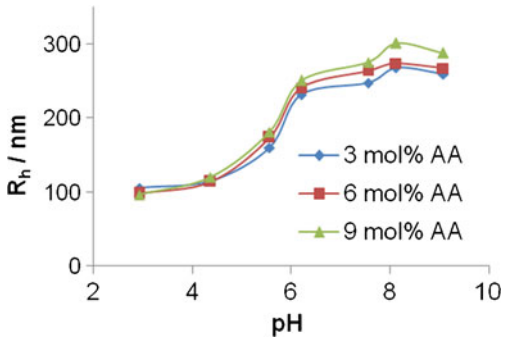

Fig. 5 pH dependence of average values of R_h of pure microgels with different feeding amount of AA at T=20 °C

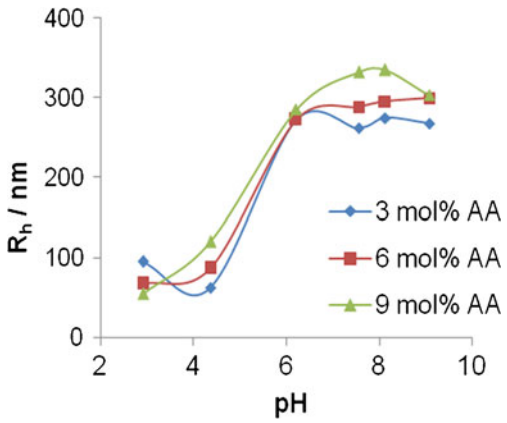

Fig. 6 pH dependence of average values of R_h of pure microgels with different feeding amount of AA at T=50 °C

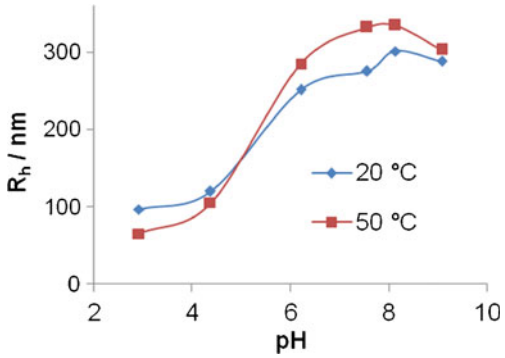

Fig. 7 pH dependence of average values of R_h of pure microgels (MG03) at two different temperature conditions of 20 °C and 50 °C

temperature accelerated the hydrolyzed reaction of amide groups [28, 38]. The comparative graph of pH sensitivity of one of the compositions at two different temperatures is shown in the Fig. 7. (See also the Figure S1 of supporting information)

Temperature sensitivity of hybrid microgels at pH=2.9

Figure 8 shows the comparative graphs of thermally induced volume phase transitions between pure microgels and hybrid gels at pH=2.9. The size of hybrid gels decreases as compared to pure microgels in all the samples. This decrease in particle size as compared to pure microgels may be due to the interaction between metal nanoparticles and polymer network. These electrostatic interactions are due to strong complexation of Ag NPs with AAm fragment in the microgels network [36, 39]. These interactions influence the ability of polymer chains to swell freely at low temperatures and results in the shrinkage of hybrid particles. So, the nanoparticles act as physical cross linkers in the microgels network. However, at pH=2.9 due to increased hydrophobicity of protonated AA units there is no significant decrease in the size of hybrid gel particles. The experimental results also indicate that transition from swollen to collapsed state become somewhat broader and less prominent due to the incorporation of Ag NPs in the microgels network [39]. This effect can be the consequence of partial charge compensation inside the polymer network due to the incorporation of Ag NPs [40]. The VPTT also undergoes a slight decrease due to the presence of Ag NPs as compared to pure microgels. Also, due to increase in the hydrophobic interactions in the hybrid gels, aggregation occurs at lower temperature and the size of aggregates becomes larger than that of pure microgels network.

Temperature sensitivity of hybrid microgels at pH=4.3

Figure 9 shows comparative graphs of pure microgels and hybrid gels at pH=4.3. At pH=4.3, the size of hybrid

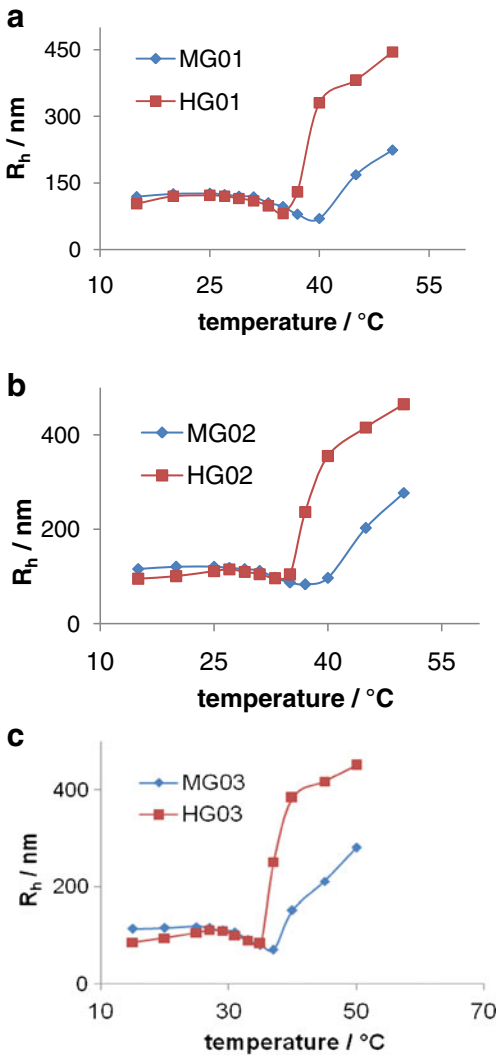

Fig. 8 Variation of average hydrodynamic radius, R_h of pure and microgels and hybrid gels at pH=2.9: **a** MG01 and HG01; **b** MG02 and HG02; **c** MG03 and HG03

microgels increases as compared to hybrid gels at pH=2.9. However, the size of hybrid gels is smaller than that of pure microgels particles. This decrease in size is due to the decrease in the electrostatic repulsions between partially ionized AA groups due to the presence of Ag NPs inside the microgels network. The experimental results show that hybrid gels show nearly the same swelling behavior as that of pure microgels. A two-step volume phase transition is also observed in hybrid system with high AA content. There is no very sharp decrease in VPTT due to the presence of Ag NPs in all the compositions.

Temperature sensitivity of hybrid microgels at pH=8.2

The comparative graphs of pure microgels and hybrid gels at pH=8.2 are shown in Fig. 10. At pH=8.2, AA groups are totally ionized. No volume phase transition is observed in

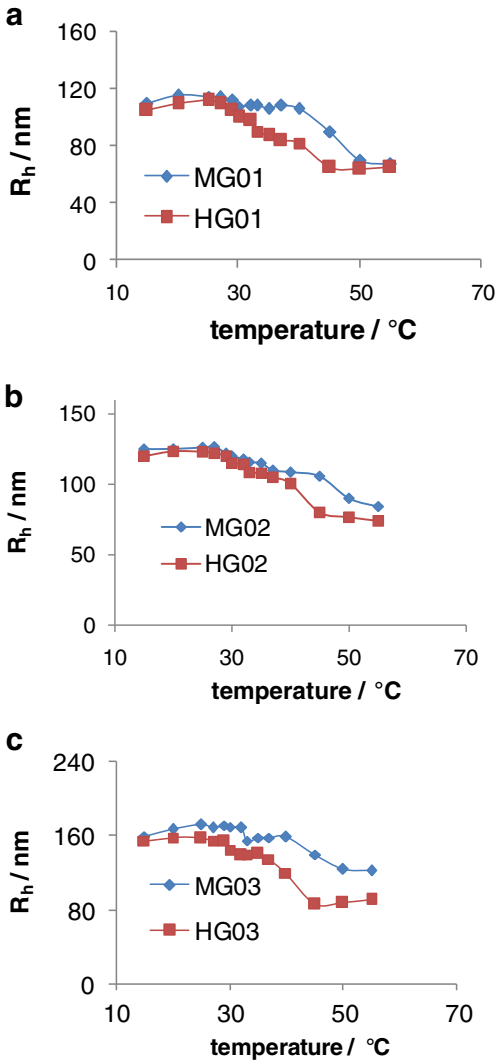

Fig. 9 Variation of average hydrodynamic radius, R_h of pure microgels and hybrid gels at pH=4.3: **a** MG01 and HG01; **b** MG02 and HG02; **c** MG03 and HG03

the studied temperature range of 15–55 °C in both pure and hybrid gels. However, the size of hybrid gel particles is significantly smaller than that of pure microgels in all the compositions.

UV–vis absorption properties of p(NIPAM-AA-AAm) hybrid gels at pH=4.3

Figure 11 shows the temperature sensitive UV–vis absorption properties of p(NIPAM-AA-AAm) hybrid gels at pH=4.3. The solution of colloidal Ag NPs has distinctive color arising from their tiny dimensions. The Ag NPs primarily absorb blue light, leaving red and green light combined to give dispersions a yellow color. At nanometer scale the electron cloud oscillate on the surface of particle and absorb electromagnetic radiation at a particular energy. This resonance known as surface plasmon resonance (SPR) is a consequence of the small size but it can also be influenced by environmental factors. The shape of SPR spectrum is determined by relative dimensions of the particle to the wavelength of incident light. Also, the variation in the refractive index of surrounding medium can change the position and intensity of resonance peaks. For example, the silica shell thickness could change the surface plasmon resonance condition of embedded Au NPs due to the changes in the local refractive index in surrounding medium [41].

The experimental results indicate that as we increase the temperature from 15 to 50 °C, the surface plasmon absorption intensity increases. The increase in absorbance starts from 35 °C. However, this increase in the absorbance is more significant in the range of 40–45 °C in case of HG03 due to two-step volume phase transition which corresponds

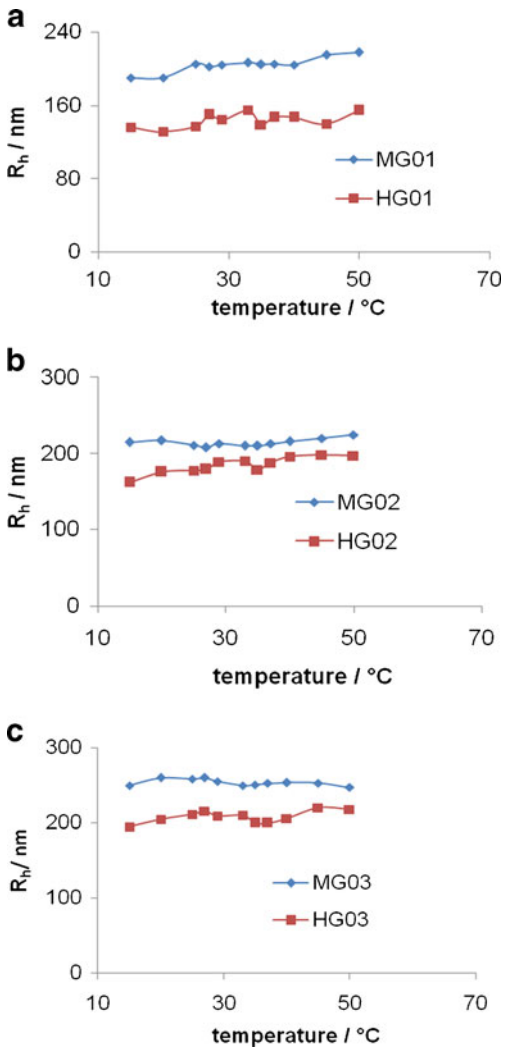

Fig. 10 Variation of average hydrodynamic radius, R_h of pure microgels and hybrid gels at pH=8.2: **a** MG01 and HG01; **b** MG02 and HG02; **c** MG03 and HG03

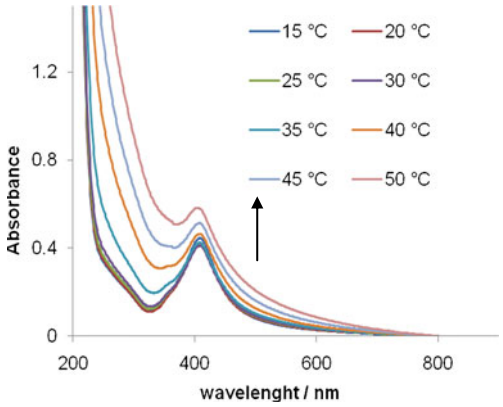

Fig. 11 Temperature sensitive UV–vis absorption properties of hybrid gels (HG03) at pH=4.3

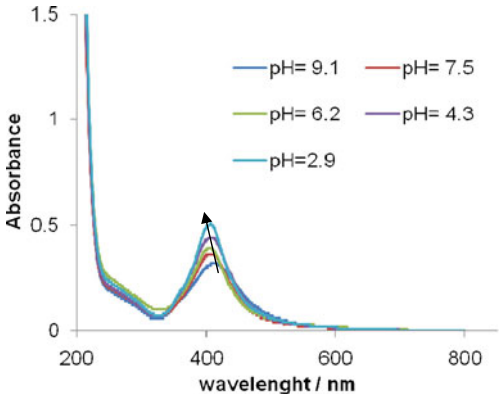

Fig. 13 pH sensitive UV–vis absorption spectrum of hybrid gels (HG03) at 25 °C

to DLS results at pH=4.3. This increase is associated with the decrease in the size of hybrid gels at higher temperatures. The concentration per unit volume ratio of Ag NPs in the hybrid gel particles increases. However, this increase is not followed by the shift in SPR band position because of the sufficient separation between the Ag NPs provided by the microgels network and the prevention of inter-particle plasmon coupling [40]. These results also correlate with the DLS results at pH=4.3. No aggregation of hybrid gel particles is observed at higher temperatures. Because of this there is no shift in SPR band position. Similar results were also observed for HG01 and HG02 (Figure S2 of supporting information)

Figure 12 shows the temperature sensitive UV–vis spectra of p(NIPAM-AA-AAm) hybrid gels with different AA amount at pH=4.3. In order to see the effect of AA content on the UV–vis absorption properties, we compare the UV–vis absorption spectra of the 3 samples at a particular temperature of 25 °C. The results indicate that by increasing the AA content, the SPR absorption intensity increases. The higher the AA content, the higher will be the affinity of Ag^{+1} ions to the microgels. This results in an increase in the concentration of Ag NPs in the microgels [42].

pH sensitive UV–vis absorption properties of p(NIPAM-AA-AAm) hybrid gels

Figure 13 shows the pH sensitive UV–vis absorption properties of p(NIPAM-AA-AAm) hybrid gel (HG03) at 25 °C. The results indicate that as the pH of the external medium was decreased from 9.1 to 2.9, an increase in the absorption intensity and a blue shift of surface plasmon bands were observed. The increase in the absorption intensity is due to the increase in the refractive index of the medium surrounding the Ag NPs [37, 41]. The pH-induced blue shift can be explained from the merging of the particle's surface charge over a small surface area so that surrounding medium cannot effectively compensate the restoring force. As a result, the electronic oscillations speed up [36, 43]. All these factors result in the increase of Rayleigh scattering as predicted by Mie theory. So, the surface polarization is the most important factor in determining the frequency and the intensity of

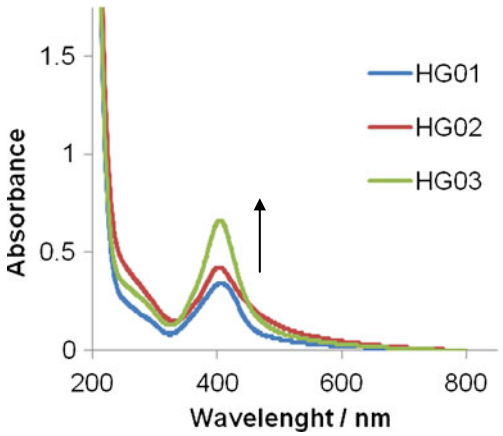

Fig. 12 Comparative temperature sensitive UV–vis spectra of hybrid gels with different AA amount at pH=4.3

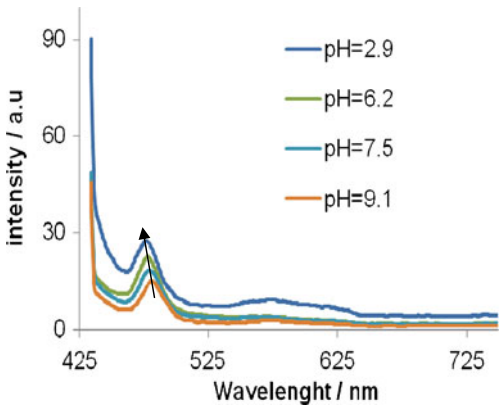

Fig. 14 pH sensitive PL spectrum of hybrid gels with 9 mol% AA at 25 °C

a given metal. HG01 and HG02 also give the similar results (Figure S3 of supporting information)

pH sensitive PL properties of p(NIPAM-AA-AAm) hybrid gels

Figure 14 shows the typical pH sensitive PL spectra of HG03 hybrid gels. The fluorescence from noble metal NPs originates from radiative recombination of sp-band electrons and the d-band holes, which could be enhanced due to the surface plasmons of nanocrystals or rough metal surfaces [36]. However, there is no PL for large metal particles, in which radiation-less processes compete with radiative processes. PL spectra for all the hybrid gels at different pH values were collected at 25 °C. The results show that there is an increase in fluorescence intensity and a blue shift of maximum emission wavelength for the peaks centered at around 470 nm. These results also correspond to pH sensitive UV–vis absorption properties of hybrid gels. The broader peaks in near IR- region might be due to the non-uniform size of Ag NPs as well as special embedding medium [44]. The pH-sensitive PL property depends on the bonding interactions between ligand molecules and the metal surface and the nonradioactive energy loss paths [36]. The increase in PL emission and the blue shift of maximum emission wavelength is due to the Ag-N bond's electron donation to the Ag NPs [36, 45]. The pH-induced swelling/deswelling of the microgels network can lead to the change in Ag-N bonding interactions. Moreover, different nonradioactive energy loss paths, related to the reduction of number surface defects, also cause the PL enhancement during microgels shrinking [36]. Such well-defined tunable pH-sensitive emission shows that the energy states involved in nanoparticle luminescence are perturbed by the surroundings to the surface of particle and the chemical characteristics of that surface. (See Figure S4 of supporting information)

Conclusion

We reported the characterization of p(NIPAM-AA-AAm) terpolymer microgels and hybrid gels with different AA content. Our results showed that at pH=2.9, both VPTT and the extent of shrinking decreases with the increase in AA content, however, at higher pH values transition becomes flatter and there is an increase in VPTT with the increase in AA groups. Ag NPs synthesized in the microgels network by in-situ reduction method were found to be fluorescent. Also, temperature sensitive UV–vis absorption studies of hybrid gels showed an increase in absorbance with the increase in temperature. The pH-sensitive UV–vis absorption studies showed an increase in the absorption intensity and a blue shift of surface plasmon bands with the decrease in pH. Also, the pH-induced shrinkage of polymer networks results in an increase in fluorescence intensity and a blue shift of maximum emission wavelength for the peaks centered at around 470 nm. Our result suggests that these smart hybrid microgels with pH-responsive PL properties may find important applications in biomedical and electronic devices.

Acknowledgements The authors gratefully acknowledge the financial support from the project funded by the Higher Education commission under the PAK-US, Pakistan Science and Technology Cooperative Program.

References

1. Smith AM, Duan H, Mohs AM, Nie S (2008) Adv Drug Delivery Rev 60:1226–1240
2. Park K, Lee S, Kang E, Kim K, Choi K, Kwon IC (2009) Adv Funct Mater 19:1553–1566
3. McCarthy JR, Weissleder R (2008) Adv Drug Delivery Rev 60:1241–1251
4. Schultz S, Smith DR, Mock JJ, Schultz DA (2000) Proc Natl Acad Sci U S A 97:996–1001
5. Han M, Gao X, Su JZ, Nie S (2001) Nat Biotechnol 19:631–635
6. Homola J, Yee SS, Gauglitz G (1999) Sens Actuators B 54:3–15
7. Tomasulo M, Yildiz I, Raymo FM (2006) J Phys Chem B 110:3853–3855
8. Filali M, Meier MAR, Schuber US, Gohy JF (2005) Langmuir 21:7995–8000
9. Lu Y, Mei Y, Drechsler M, Ballauff M (2006) Angew Chem Int Ed 45:813–816
10. Pich A, Karak A, Lu Y, Ghosh AK, Adler HJ (2006) Macromol Rapid Commun 27:344–350
11. Orakdogen N (2012) J Polym Res 19:9914–9924
12. Liu Q, Li S, Zhang P, Lan Y, Lu M (2007) J Polym Res 14:397–400
13. Biffis A, Orlandi N, Corain B (2003) Adv Mater 15:1551–1555
14. Biffis A, Minati L (2005) J Catal 236:405–409
15. Ionov L, Sapra S, Synytska A, Rogach AL, Stamm M, Diez S (2006) Adv Mater 18:1453–1455
16. Tokareva I, Minko S, Fendler JH, Hutter E (2004) J Am Chem Soc 126:15950–15951
17. Suzuki D, Kawaguchi H (2006) Langmuir 22:3818–3822
18. Kim MH, Kim JC, Lee HY, Kim JD, Yang JH (2005) J Colliod Surface B 46:57–61
19. Anastasiadis SH, Vamvakaki M (2009) Int J Nanotechnol 6:46–70
20. Ballauff M, Lu Y (2007) Polymer 48:1815–1823
21. Zhang J, Xu S, Kumacheva E (2004) J Am Chem Soc 126:7908–7914
22. Gong Y, Gao M, Wang D, Mohwald H (2005) Chem Mater 17:2648–2653
23. Li J, Hong X, Liu Y, Li D, Wang Y, Li J, Bai Y, Li T (2005) Adv Mater 17:163–166
24. Zhang J, Xu S, Kumacheva E (2005) Adv Mater 17:2336–2340
25. Shibayama M, Mizutani S, Nomura S (1996) Macromolecules 29:2019–2024
26. Seno M, Len ML, Iwamoto K (1991) Colloid Polym Sci 269:873–879
27. Farooqi ZH, Khan A, Siddiq M (2011) Polym Int 60:1481–1486
28. Lee W, Shieh C (1999) J Appl Polym Sci 71:221–231

29. Kratz K, Hellweg T, Eimer W (2000) Colloids and Surf A: Physiochem Eng Aspects 170:137–149
30. Kim KS, Kim MH, Cho SH (2005) Ind Eng Chem 11:736–742
31. Zhou S, Chu B (1998) J Phys Chem B 102:1364–1371
32. Farooqi ZH, Wu W, Zhou S, Siddiq M (2011) Macromol Chem Phys 212:1510–1514
33. Flory PJ (1953) Principles of Polymer Chemistry. Cornell University Press, London
34. Cesarano J, Aksay IA, Bleier A (1988) J Am Ceram Soc 71:250–255
35. Zhang Y, Guan Y, Zhou S (2006) Biomacromolecules 7:3196–3201
36. Wu W, Zhou T, Zhou S (2009) Chem Mater 21:2851–2861
37. Wu W, Zhou T, Berliner A, Banerjee P, Zhou S (2010) Chem Mater 22:1966–1976
38. Khare AR, Peppas NA (1995) Biomaterials 16:559–567
39. Xu H, Xu J, Zhu Z, Liu H, Liu S (2006) Macromolecules 39:8451–8455
40. Pich A, Karak A, Lu Y, Ghosh AK, Adler HP (2006) Macromol Rapid Commun 27:344–350
41. Marazan LL, Giersig M, Mulvaney P (1996) Langmuir 12:4329–4335
42. Zhang J, Xu S, Kumacheva E (2004) J Am Chem Soc 126:7908–7914
43. Underwood S, Mulvaney P (1994) Langmuir 10:3427–3430
44. Felix C, Sieber C, Harbich W, Buttet J, Rabin I, Schulze W, Ertl G (1999) Chem Phys Lett 313:105–109
45. Huaung T, Murray RW (2003) J Phys Chem B 107:7434–7440